



ELSEVIER

Nuclear Instruments and Methods in Physics Research B 136–138 (1998) 1345–1348

NIM B
Beam Interactions
with Materials & Atoms

Fluence dependence of IBIC collection efficiency of CMOS transistors

T. Osipowicz ^{a,*}, J.L. Sanchez ^a, I. Orlic ^a, F. Watt ^a, S. Kolachina ^b, D.S.H. Chan ^b,
J.C.H. Phang ^b

^a Nuclear Microscopy Group, Physics Department, National University of Singapore, Kent Ridge, Singapore 119260, Singapore

^b Centre for Integrated Circuit Failure Analysis and Reliability, National University of Singapore, Kent Ridge, Singapore 119260, Singapore

Abstract

IBIC (Ion Beam Induced Charge) imaging of deep structures of semiconductor devices with a focused MeV light ion beam has been shown to offer significant advantages over the established EBIC (Electron Beam Induced Current) technique, because the large range and the small lateral straggling of the ion beam allows direct imaging of buried device structures. The technique is limited by the accumulation of radiation damage that reduces the charge collection efficiency. We report on measurements of the beam fluence dependence on IBIC collection efficiency for proton and alpha particle beams at 2000 keV energy. A HCF4007 CMOS transistor array was used in these measurements. The influence of surface passivation layers on charge collection efficiency and its evolution with ion dose is discussed. © 1998 Elsevier Science B.V.

Keywords: Microbeam; Charge microscopy; Device imaging

1. Introduction

As the number of multi-level designs in the production of microelectronic circuits increases, Ion Beam Induced Charge (IBIC) microscopy promises to be a powerful tool for the analysis of buried structures in semiconductor devices [1]. Most of the work done in the field has dealt with the analysis of microelectronics devices [2–5] and charac-

terization of materials, e.g., diamond-like carbon thin films [6].

For applications in microelectronics the accumulation of radiation damage presents a serious limitation of the IBIC technique. It has been shown that IBIC charge collection efficiencies decrease steeply as the ion beam dose increases, depending on the device geometry and beam type and energy. Breese et al. [7] have reported calculations where the evolution of IBIC pulse height is treated in terms of a one-dimensional model that incorporates diffusion of charge to the collection junction and the creation of defects that act as recombination and trapping centers along the path

*Corresponding author. Tel.: +65 772 6745; fax: +65 777 6126; e-mail: phyto@leonis.nus.sg.

of the incident ion. This paper presents laterally resolved IBIC pulse height spectra for 2 MeV H^+ and He^+ ions as a function of the ion dose for a CMOS device.

2. Experimental

The measurements were carried out at the National University of Singapore Nuclear Microscopy facility [8]. The ion beam from the van de Graaff accelerator is focused to produce a beam spot of around $1\ \mu\text{m}$ size. The object and collimator aperture settings are then suitably adjusted to reduce the beam intensity to ~ 1000 ions/s, the current being determined from the count rate of a surface barrier STIM detector. The device to be imaged is connected to an OMDAQ nuclear electronics data acquisition system with a charge sensitive ORTEC 142A preamplifier [8]. Calibration of the pulse height spectra is achieved by the accumulation of an RBS spectrum of a calibrated sample with the same electronic setup. Event by event data acquisition is employed, allowing for off-line data analysis. The IBIC images are constructed on-line in map-mode, displaying the intensity of the pulses from windows in the charge collection spectra. However, better contrast is found to be present in off-line generated images that represent the mean value of the charge collection spectrum for each pixel. All images presented here were generated using the latter procedure. The OMDAQ software package also allows spectra for predefined areas to be sorted, thereby extracting collection efficiency spectra for specific regions of a device. The events are stored sequentially, therefore it is possible to restrict the sorting procedure to sequential intervals. This feature allows deduction of the dose dependence of the charge collection efficiency.

3. CMOS IBIC damage

The dose dependence of the IBIC collection efficiency was measured for a CMOS transistor array. An optical micrograph and a schematic cross section of one of the transistors in the p-well

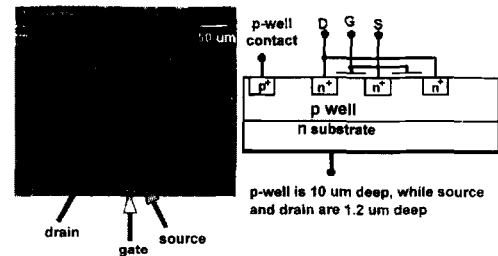


Fig. 1. Optical micrograph of the n-channel transistor. The diagram represents the available contacts.

is shown in Fig. 1. The p-well has a depth of $10\ \mu\text{m}$, and the source and drain regions are $1.2\ \mu\text{m}$ deep. A $3.3\ \mu\text{m}$ SiO_2 passivation layer covers the surface except for the contact regions. The n-substrate/p-well junction is connected to the preamplifier in the measurements presented here.

Fig. 2 shows the initial IBIC image generated with a 2 MeV proton beam. The boxed region contains a CMOS transistor in the p-well, as shown in Fig. 1. The image contrast stems mainly from the p-well/n-substrate junction, the collecting junction. Some contrast is generated at the transistors via the unconnected junction contrast mechanism as described in [9]. The surface topology, e.g. the presence of metal lines or changing oxide thicknesses is not visible due to the relatively low rate of energy loss ($29\ \text{keV}/\mu\text{m}$ in SiO_2 [10]) of the proton beam at the surface. Fig. 2 also shows the IBIC pulse height as a function of the ion dose, for the boxed region in Fig. 2 which covers one of the transistors. A dose dependence consistent with previous results [2] is measured.

Fig. 3 displays an IBIC image of the p-well transistor shown in Fig. 1. A 2 MeV He^+ beam was used to generate the image. The relatively large energy loss of the He ions ($275\ \text{keV}/\mu\text{m}$ in SiO_2 [10]) at the surface renders the surface structures visible. Aluminum metal lines are visible, as well as the boundary of the collecting junction. The transistor junctions are also faintly visible. Fig. 4 shows the dose dependence of the IBIC pulse height for the five regions indicated. The initial IBIC collection efficiency varies between 757 and 392 keV, mainly due to different surface layer thicknesses. The largest collection is seen in region 1, where only the oxide passivation layer is present

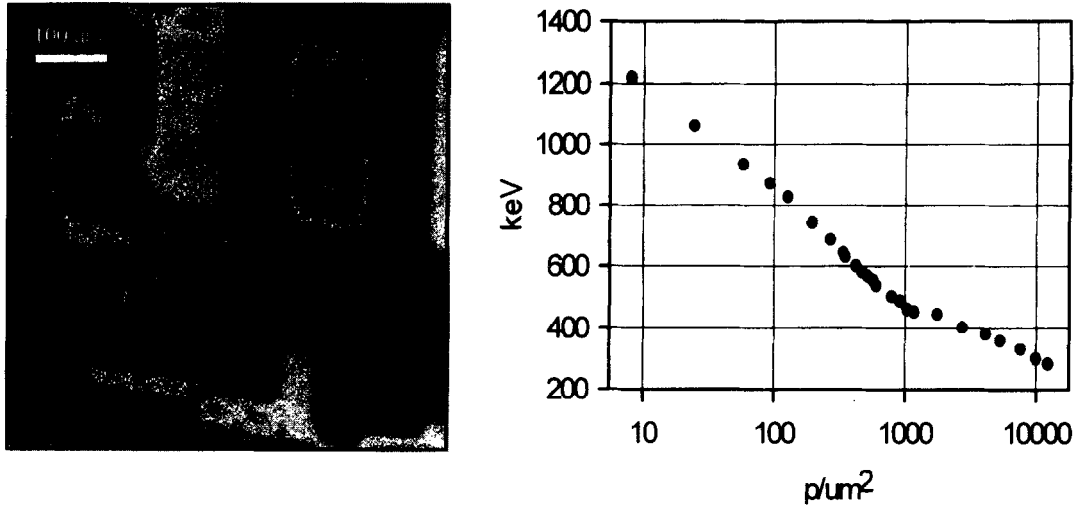


Fig. 2. Low dose ($5 \text{ p}/\mu\text{m}^2$) IBIC image of an n-channel transistor, generated with a 2 MeV proton beam. The IBIC efficiency evolution of the boxed region is shown in the graph.

above the collecting junction. The ion range is shorter than the p-well/n-substrate junction, and peak of the radiation damage is in the field-free region above the junction, resulting in the observed rapid decrease in charge collection. In region 5, an additional SiO_2 surface layer is present between

the Al interconnect lines and the silicon, reducing the ion range in Silicon and hence the initial IBIC efficiency. The steep decrease in IBIC efficiency is again due to beam damage. However, at the regions 2-4 nearly constant IBIC efficiencies are observed. The essential difference between regions 1, 5 and 2-4 is the presence of an additional source/drain junction in regions 2-4. It is assumed that the slow efficiency decrease here is associated with these junctions. This negligible decay of the IBIC efficiency enables significantly higher beam exposures, and hence better IBIC images. Presently we are investigating these effects, which are probably related to funneling [2] or unconnected junction effects [9].

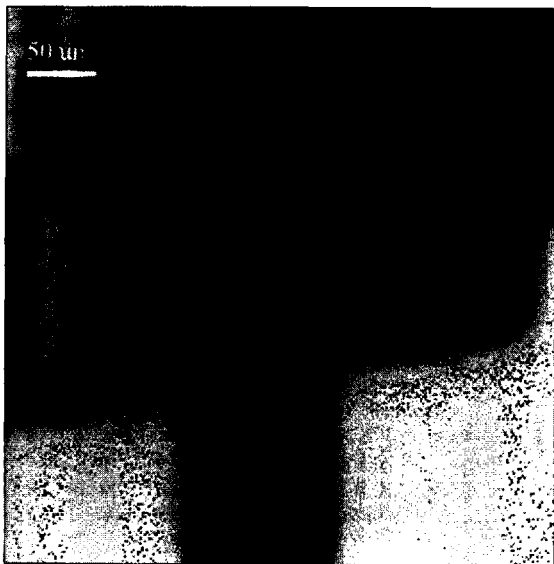


Fig. 3. IBIC image of an n-channel transistor generated with a 2 MeV He^+ beam.

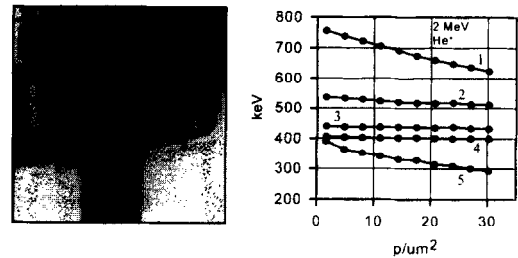


Fig. 4. IBIC image of an n-channel transistor, generated with a 2 MeV He^+ beam. The IBIC efficiency evolution of the indicated regions is shown in the graph.

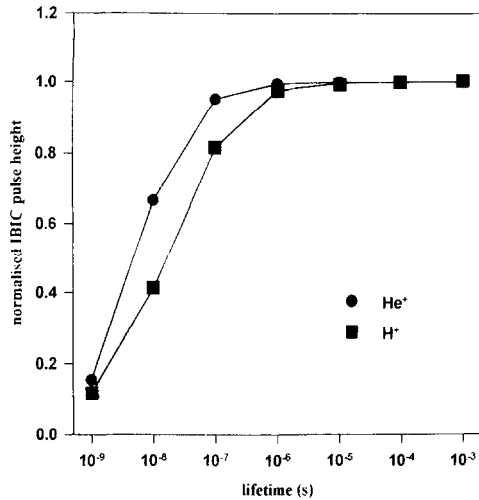


Fig. 5. MEDICI simulated normalized IBIC pulse height as a function of bulk minority carrier lifetime for 2 MeV H⁺ and He⁺ ions.

4. Device simulation for IBIC

Numerical device simulation can improve our understanding of charge collection processes taking place when an ion strikes the semiconductor devices. We are currently investigating the use of the commercially available 2-D device simulation software MEDICI for the simulation of IBIC events. This approach allows a quantitative understanding of IBIC data from devices with complex structures. The depth distribution of electron–hole pair generation can be obtained from the Monte Carlo ion transport code TRIM [10] and incorporated into the MEDICI simulation. The charge transport and diffusion equations are then solved numerically to yield time dependent excess carrier concentrations in the device. The resultant current transient is then integrated to obtain a simulated IBIC pulse height. This approach will also help to clarify the degradation-related effects in CMOS devices because degradation results in depth dependent carrier lifetime changes that can be incorporated in MEDICI. Fig. 5 shows the normalized variation of the simulated IBIC pulse height with

the bulk minority carrier lifetime in a 10 μm deep pn-junction for 2 MeV proton and 2 MeV He⁺ striking the diode. In both cases the pulse height decreases with decreasing lifetime, however the He⁺ induced pulse height starts to decrease at a lower lifetime than the proton induced pulse height.

5. Conclusion

Laterally resolved IBIC collection efficiencies from CMOS transistors were measured as a function of ion dose for 2 MeV He⁺ and H⁺ ions. No strong effect from the surface topology was seen in the H⁺ irradiations, but for He⁺ irradiation surface structures (e.g. metal lines, passivation layers) were strongly affecting the IBIC images. The influence of surface passivation layers on charge collection efficiency and its evolution with ion dose is discussed, and changes in the dose dependence, tentatively attributed to funneling, are shown.

References

- [1] M.B.H. Breese, G.W. Grime, F. Watt, Nucl. Instr. and Meth. B 77 (1993) 305.
- [2] M.B.H. Breese, D.N. Jamieson, P.J.C. King, Materials Analysis Using a Nuclear Microprobe, Wiley, New York, 1996.
- [3] K.M. Sexton, K.M. Horn, B.L. Doyle, J.S. Laird, M. Cholewa, A. Saint, G.J. Legge, Nucl. Instr. and Meth. B 79 (1993) 436.
- [4] M. Takai, Nucl. Instr. and Meth. B 113 (1996) 330.
- [5] M.B.H. Breese, P.J.C. King, G.W. Grime, F. Watt, J. Appl. Phys. 72 (1992) 2097.
- [6] C. Manfredotti, F. Fizzotti, P. Polesello, E. Vittone, P. Rossi, G. Egeni, V. Rudello, I. Bogdanovic, M. Jasic, V. Valkovic, Nucl. Instr. Meth. B 130 (1997) 491.
- [7] M.B.H. Breese, J. Appl. Phys. 74 (1993) 3789.
- [8] F. Watt, I. Orlic, K.K. Loh, C.H. Sow, P. Tong, S.C. Liew, T. Osipowicz, T.F. Choo, S.M. Tang, Nucl. Instr. Meth. B 85 (1994) 708.
- [9] S. Kolachina, V.K.S. Ong, D.S.H. Chan, J.C.H. Phang, T. Osipowicz, F. Watt, Appl. Phys. Lett. 68 (1996) 532.
- [10] J.F. Ziegler, J.P. Biersack, U. Littmark, The Stopping and Range of Ions in Solids, Pergamon, New York, 1985.